Dynamics of Tin Nuclei in Alkyltin(IV)–Deoxyribonucleic Acid Condensates by Variable-temperature Tin-119 Mössbauer Spectroscopy†

Renato Barbieri,*[a] Giuseppe Ruisi,[a] Arturo Silvestri,[a] Anna Maria Giuliani,[a] Adriana Barbieri,[a] Gabriele Spina,[b] Fabrizio Pieralli[b] and Franco Del Giallo[b]

[a] *Dipartimento di Chimica Inorganica, Università di Palermo, I-90123 Palermo, Italy*

[b] *Dipartimento di Fisica, Università di Firenze, I-50139 Firenze, Italy*

The dynamics of tin nuclei in the condensates SnR_2(DNA monomer)$_2$ and SnR_3(DNA monomer) (R = Me or Et), freeze-dried, has been investigated by variable-temperature ^{119}Sn Mössbauer spectroscopy. Linear functions $\ln(A_t/A_{77.3})(T)$, $\ln f_a^{rel,abs}(T)$ and $\langle x^2\rangle(T)$ (A_t = total area under the resonant peaks, f_a the relative and the absolute estimates of Lamb–Mössbauer factors, and $\langle x^2\rangle$ the mean-square displacements of the Mössbauer nucleus extracted from f_a^{rel} and f_a^{abs} respectively) have been found at $T \geqslant 77.3$ K, which indicate harmonic motions and the lack of phase transitions. The latter is also suggested by the temperature-invariant hyperfine parameters, isomer shift, nuclear quadrupole splitting (ΔE) and peak widths. From the slopes of the functions $\ln A_t(T)$ and $\ln f_a^{rel}(T)$, the dynamics of tin in alkyltin(IV)–DNA condensates is found to be analogous to that in organotin(IV) salts and complexes, on the assumption of effective vibrating masses, corresponding to molecular groups. The coincidence between $f_a^{rel,abs}$, as well as the related $\langle x^2\rangle$, data, indicates that the negative charge on the DNA backbone phosphodiester groups is fully neutralized by alkyltin(IV) cations in SnR_2(DNA monomer)$_2$ (R = Me or Et) as well as in $SnEt_3$(DNA monomer), while only partially in $SnMe_3$(DNA monomer) and in $SnMe_2$(DNA monomer)$_2$ obtained by standard procedures for DNA condensation. From the magnitude of the functions, as well as of the Debye temperatures, on fingerprint criteria, $Sn^{IV}R_2$ moieties are assumed to bridge phosphodiester groups in toroidal condensates through interstrand bonding, while $Sn^{IV}R_3$ would be appended to the double helix. Motions would involve SnR_2(mononucleotide)$_2$ and SnR_3(mononucleotide) units as the effective vibrating masses. Two tin co-ordination sites occur for $Sn^{IV}R_2$ moieties at the DNA surface, both *trans*-octahedral, and a single trigonal-bipyramidal site for $Sn^{IV}R_3$, the organometal moieties being co-ordinated by phosphodiester and water oxygen atoms, according to ΔE rationalization by point-charge model structure simulations, as well as to Mössbauer–Zeeman spectra of the $Sn^{IV}Et_2$– and $Sn^{IV}Et_3$–DNA condensates.

The dynamics of nucleic acids is of great interest.[1] A number of experimental techniques have been employed, such as NMR,[2] Raman,[3] EPR,[4] UV, circular dichroism spectroscopy and electron microscopy.[5] Local, as well as collective, dynamics is investigated, for example by ^{31}P and ^{15}N NMR (uniform label), as well as by deuterium NMR and EPR spectroscopy of nitroxide radicals (both labelling heterocyclic bases).[2,4] Theoretical approaches to the treatment of short-time dynamics, local structural transitions, global structural changes, and molecular associations have been reported,[1b] in the context of rapidly growing developments.[1,6]

As part of our studies on the molecular basis of the biological activity of organotin(IV) compounds,[7] we have recently reported on the formation of condensates by reaction of calf thymus DNA with dialkyl- and trialkyl-tin(IV) moieties.[8] Structure simulation by the point-charge model treatment of the ^{119}Sn Mössbauer parameter nuclear quadrupole splitting evidenced *trans*-alkyl octahedral dialkyltin(IV) units, as well as trigonal-bipyramidal trialkyltin(IV) (equatorial SnC_3), where the tin atoms would be covalently bound to phosphodiester oxygens.[8] The latter is in line with the results of studies on model systems in aqueous solution at physiological pH[9] as well as in the solid state.[10] The lattice dynamics of $SnR_2(AMP)\cdot 2H_2O$ (R = Me or Bu^n; AMP = adenosine 5′-monophosphate) studied by variable-temperature ^{119}Sn Mössbauer spectroscopy revealed a polymeric structure centred at the tin atom.[10]

† *Non-SI units employed:* Ci = 37 × 10^{10} Bq, eV ≈ 1.60 × 10^{-19} J.

These studies have now been extended to the determination of the dynamics of tin nuclei in organotin(IV)–DNA condensates by variable-temperature Mössbauer spectroscopy and the results are discussed in relation to iron-57 data concerning iron proteins, in line with actual trends.[1b] Lyophilized condensates have been investigated, where no glass transitions[11] would occur, in accord with findings for proteins.[12,13] The tin dynamics are assumed to be coupled with those of DNA fragments, analogously to results for iron proteins[12] and iron-doped polymers.[14] The structures of tin sites[8] have been checked by point-charge model calculations, as well as by the determination of the sign of the ^{119}Sn Mössbauer nuclear quadrupole splitting, ΔE, and of the value of the asymmetry parameter, η, for two representative condensates, by Mössbauer–Zeeman spectroscopy.[15]

Experimental

The condensates[8] SnR_2(DNA monomer)$_2$ and SnR_3(DNA monomer) have been obtained by the following procedures[8]: (I) SnR_nCl_{4-n} (n = 2, R = Me or Et; n = 3, R = Et) 0.1 mol dm^{-3} in EtOH was added to calf thymus DNA (13.1–19.6 mmol dm^{-3}, in monomer units) in 1 mmol dm^{-3} tris(hydroxymethyl)-aminomethane (Tris), 0.1 mmol dm^{-3} disodium salt ethylenediamine-*N*,*N*,*N*′,*N*′-tetraacetate (Na_2H_2edta), in tridistilled water, pH 8; ≈ 10% EtOH in the final mixture; r (= mmol SnR_n per mmol DNA monomer) = 0.5 for SnR_2 and = 1.0 for $SnEt_3$; immediate formation of condensates takes place for $SnEt_2$ and $SnEt_3$, while slow precipitation of the gelled phase occurs for

$SnMe_2$; (II) $SnMe_2Cl_2$ 0.1 mol dm^{-3} in EtOH, $r = 0.5$, was added to calf thymus DNA as described above; pellets were obtained by addition of NaCl (0.1 mol dm^{-3} in the final mixture) and two to three volumes of EtOH; (III) $SnMe_3Cl$ 0.1 mol dm^{-3} in water was added to calf thymus DNA (as above), $r = 2.5$; gelled phases were obtained by addition of HCl till pH $\approx$ 3; (IV) $SnMe_3Cl$ 0.1 mol dm^{-3} in EtOH was added to calf thymus DNA (as above), $r = 2.5$, $\approx$ 30% EtOH in the final mixture; a gelled phase was formed.

Pellets from methods (I)–(IV) were recovered by centrifugation, and freeze-dried with Heto (Denmark) lyophilizers. The preparations are detailed in Table 1. The reported stoichiometries of the condensates were assigned from the determination of the percentage ^{119}Sn Mössbauer resonant effect, ε, in pellets and supernatants.[8]

The products employed in the present study were obtained commercially. The alkyltin chlorides were from ICN Biomedical (Plainview, USA) and Aldrich Italia (Milan, Italy). The compounds were eventually recrystallized [$SnMe_2Cl_2$ from benzene, $SnMe_3Cl$ and $SnEt_2Cl_2$ from light petroleum (b.p. 40–70 °C)] and their purities checked by melting and boiling points (the latter for $SnEt_3Cl$).[16,17] Tris was from Sigma (St. Louis, MO, USA), and other reagents and solvents from C. Erba (Milan, Italy).

The Mössbauer (nuclear gamma resonance) spectra were recorded with conventional spectrometers operating in the transmission mode. The source was $Ca^{119}SnO_3$ (Radiochemical Centre, Amersham; 10 mCi), moving at room temperature with constant acceleration in a triangular waveform. The emitted non-resonant tin kX radiations were filtered out by a palladium foil 0.05 mm thick.[18] Appropriate lead shielding was employed. The variable-temperature spectra, at $T \geqslant 77.3$ K, were recorded using a MVTIN 200 sample holder, a CTC 200 temperature controller and a MNC 200 liquid-nitrogen cryostat, from AERE (Harwell, UK), the temperature being measured with a chromel–alumel thermocouple (stabilized to ± 0.5 K). Measurements were also carried out with a sample holder and a DTC 200 temperature controller equipped with a Pt-100 sensor, from Finder (Lübeck, Germany). The driving system was from Halder (Seehausen, Germany), and the NaI(Tl) detector from Harshaw (De Meern, Holland). Multichannel analysers and the related electronics were from Laben (Milan, Italy; model 4000) and Takes (Bergamo, Italy; model 269). Very narrow windows for the 23.87 KeV ^{119}Sn γ-rays were selected in the analysers.

At $T \geqslant 15$ K measurements were effected with a cryogenerator-cooled cryostat. In the apparatus[19] the source is bonded to the transducer moving shaft while the sample holder is secured to the external body of the driver. A flexible copper plait transports heat from the holder to the cryogenerator second stage. Owing to its flexibility and peculiar mechanical arrangement, vibrations do not affect the collected spectrum.[19] In order to secure temperature uniformity till 15 K, the sample holder is thermally shielded by a box connected to the first stage of the cryogenerator. The sample holder is made from copper and thermally stabilized by an electric heater bonded to the copper plait. The temperature is measured by a Rh(Fe) sensor. The system is kept stable to within ± 0.1 K. As the whole apparatus must operate under vacuum and the cryogenerator vibrates, the cryostat body and the motor, source and absorber are connected through a metallic bellows and a suitable vibration dumper.

The Mössbauer–Zeeman spectra[15] were recorded in an applied longitudinal magnetic field. The superconducting magnet, cooled by liquid He, can generate fields up to 5 T. The sample holder was mounted in a vacuum chamber, thermally shielded and placed in the hole of the magnet. The temperature was controlled by the helium flux and an electrical heater. The magnetic field acts only on the sample; the field acting on the source is zero due to an opposed sign-balancing field. Aluminized mylar windows function also as heat shields, but allowing the passage of gamma radiation.

Data reduction was effected by fitting the experimental spectra by Lorentzian lineshapes, using programs based upon iterative non-linear least-squares analysis[20] (*e.g.* the NORMOS program for two-doublet fitting). Calibration was effected with spectra from $Ca^{119}SnO_3$ and ^{57}Fe, the standard errors being: zero point, ± 0.001 mm s^{-1}; g_0, ± 0.0291 mm s^{-1}; g_1, ± 0.0166 mm s^{-1}. The alkyltin(IV)–DNA freeze-dried condensates (Table 1) were employed as absorber samples ('thin' according to the content of ^{119}Sn) without further treatment, as discs in aluminium foils, fixed with Scotch Tape and mounted on the sample holders. The quality of the spectra is shown in Fig. 1.

Results and Discussion

Dynamics from the 'Relative' Recoil-free Fraction and Trends in the Hyperfine Parameters.—The dynamics of tin nuclei in alkyltin(IV)–DNA condensates was investigated through the determination of the temperature dependence of the Lamb–Mössbauer factor f_a.[21] The treatment of data previously described[22] was essentially followed. For Debye solids in the high-temperature limit ($T \geqslant \theta_D/2$), 'relative' f_a values are calculated from the slope of the function total area under the resonant peaks, A_t, *vs.* temperature [equation (1)] where E_γ is

$$\frac{d \ln A_t}{dT} = \frac{d \ln f_a}{dT} = \frac{-3E_\gamma^2}{Mc^2k\theta_D^2} \quad (1)$$

the energy of the Mössbauer transition, M the mass of the vibrating atom or molecular unit (the latter taken as the effective vibrating mass), k the Boltzmann constant, and θ_D the

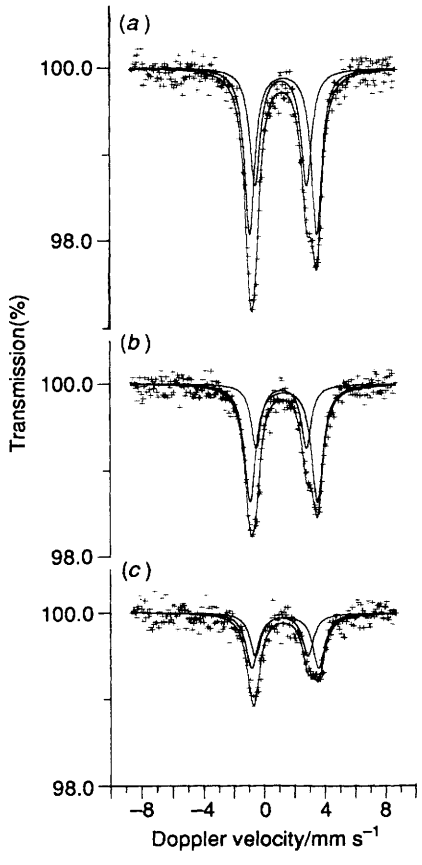

Fig. 1 Quality of the ^{119}Sn Mössbauer spectra obtained, and the occurrence of two distinct co-ordination sites at tin, as shown by the fitting of experimental data points by two symmetric Lorentzian doublets, for the condensate $SnMe_2(DNA\ monomer)_2$ (series 1, Table 1) at 77.3 (*a*), 120 (*b*) and 172 K (*c*)

Table 1 Preparation of $Sn^{IV}R_n$–DNA condensates, and their compositions from 'gravimetry' and ^{119}Sn Mössbauer spectroscopy

			SnR_nCl_{4-n}		DNA	Lyophilized condensate			Mössbauer data	
No.	Condensate[a] (formula weight)[b]	Method of preparation[c]	μmol	mg ^{119}Sn[d]	monomer (μmol)	mg	mg ^{119}Sn[d,e]	10^{17} N[e,f]	10^{17} N[f,g]	No. of data points (T range/K)[h]
1, 2	$SnMe_2$(DNA monomer)$_2$ (778.76)	I	75	0.76	150	32.5	0.43	21.6	20.8, 26.4	16 (77.3–280)
3		II	75	0.76	150	73.6	0.96	48.8	8.76	8 (77.3–293)
4, 5	$SnMe_3$(DNA monomer) (478.79)	III	750	7.63	298	20.9	0.44	22.5	8.57, 8.61	21 (77.3–160)
6, 7		IV	375	3.82	150	55.7	1.18	60.1	16.5, 19.8	14 (77.3–220)
8, 9	$SnEt_2$(DNA monomer)$_2$ (806.81)	I	72	0.73	144	61.9	0.78	39.6	40.8	20 (15–288)
10, 11		I	72	0.73	144	57.5	0.73	36.8	41.4, 41.5	9 (77.3–210)
12, 13		I	72	0.73	144	48.0, 51.0	0.61, 0.64	30.7, 32.7	28.8, 32.3	13 (77.3–269.5)
14, 15	$SnEt_3$(DNA monomer) (520.88)	I	131	1.33	131	59.3	1.16	58.8	66.1	20 (15–200)
16		I	131	1.33	131	56.9	1.11	56.4	56.4	14 (77.3–221)

[a] Stoichiometries from ^{119}Sn Mössbauer data[8] (see text). [b] Calculated by assuming M = 315 for DNA monomer unit. [c] See text, Experimental section. [d] Calculated from the natural abundance of ^{119}Sn, 8.58%. [e] Calculated from the mg of the obtained freeze-dried sample, assuming the indicated stoichiometry and formula weight. [f] N is the total number of ^{119}Sn atoms. [g] Calculated from equation (3) by assuming $f_a^{rel} = f_a^{abs}$; average data over the corresponding temperature ranges (see text). Each figure refers to one series of variable-temperature measurements, using the apparatus described in the Experimental section. [h] The total number of spectra determined; the spectra employed in the molecular dynamics treatment range from T = 77.3 K to T_{max} for each series. See Fig. 2.

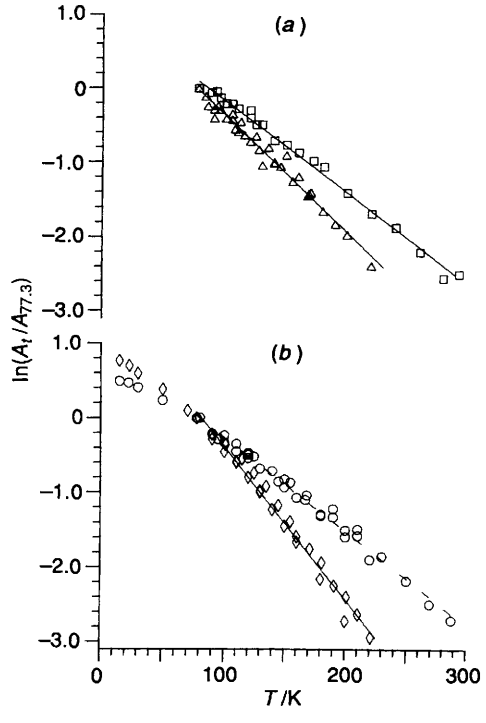

Fig. 2 Functions $\ln(A_t/A_{77.3})$ *vs.* T for $Sn^{IV}R_2$– and $Sn^{IV}R_3$–DNA condensates, freeze-dried; $A = (\pi/2)\varepsilon\Gamma$ is the total Lorentzian area under the ^{119}Sn Mössbauer peaks (ε = percentage effect; Γ = full width at half-height of the resonant peaks). All data points determined are reported, for the variable-temperature sets 1–16, Tables 1 and 2. Lines are least-squares fits $y = ax + b$ where slopes a are in Table 2 and intercepts b are as follows (data refer to T 77.3–T_{max} for each series): (*a*) (□) $SnMe_2$(DNA monomer)$_2$, 1.040; (△) $SnMe_3$(DNA monomer), 1.179; (*b*) (○) $SnEt_2$(DNA monomer)$_2$, 0.986; (◇) $SnEt_3$(DNA monomer), 1.662

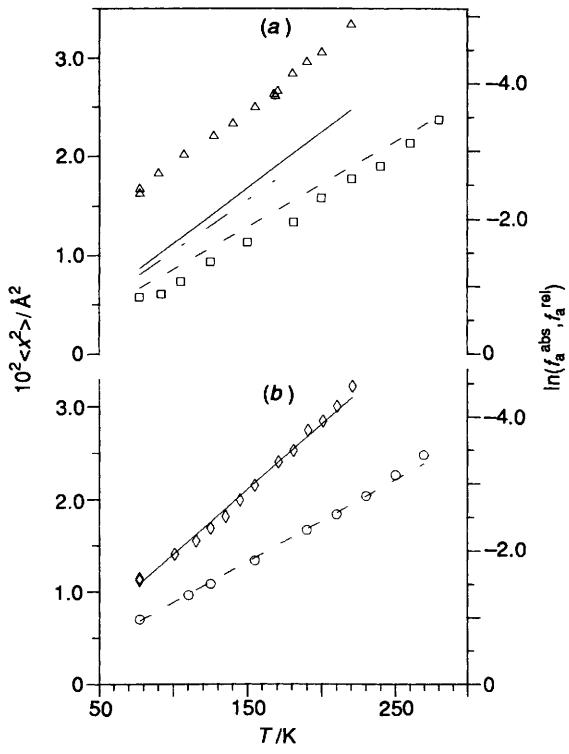

Fig. 3 Recoil-free fractions of the absorber ^{119}Sn nuclei, f_a, and mean-square displacements of ^{119}Sn, $\langle x^2\rangle$, as a function of temperature, for representative samples of $Sn^{IV}R_2$– and $Sn^{IV}R_3$–DNA condensates, freeze-dried, and related series of variable-temperature measurements (listed in Tables 1 and 2). Lines are plots of f_a^{rel}, and the related $\langle x^2\rangle$ functions as extracted from the slopes d ln A_t/dT while data points are 'absolute' data, f_a^{abs}, and corresponding $\langle x^2\rangle$. (*a*) $SnMe_2$(DNA monomer)$_2$, series 2, (- - -) f_a^{rel}, $\langle x^2\rangle$; (□) f_a^{abs}, $\langle x^2\rangle$; $SnMe_3$-(DNA monomer), series 6 and 7, (— and — · —) f_a^{rel}, $\langle x^2\rangle$; (△) f_a^{abs}, $\langle x^2\rangle$. (*b*) $SnEt_2$(DNA monomer)$_2$, series 13, (- - -) f_a^{rel}, $\langle x^2\rangle$; (○) f_a^{abs}, $\langle x^2\rangle$; $SnEt_3$(DNA monomer), series 16, (——) f_a^{rel}, $\langle x^2\rangle$; (◇) f_a^{abs}, $\langle x^2\rangle$

Debye temperature. The functions A_t *vs.* T are extrapolated to $T = 0$ K, and f_a^{rel} is defined as in equation (2) where A_0 is the estimated area at 0 K, *i.e.* $f_a = 1$ at 0 K.

$$f_a^{rel}(T) = (A_t/A_0)(T) \qquad (2)$$

Data points for the series of the four classes of alkyltin(IV)–DNA condensates investigated in the present study, 1–16 in Table 1, are reported in Fig. 2; normalization to 77.3 K within each series yields individual total functions ln $A(T)$ for any of the four types of condensates. The functions appear to be linear at $T \geqslant 77.3$ K (according also to the correlation coefficients in Table 2), obviously reflecting trends in $\ln f_a^{rel}(T)$, as represented in Fig. 3. Consequently, no glass transition[11] occurs for the freeze-dried DNA condensates, eventually expected around 200 K, which is in accord with findings for lyophilized iron proteins.[12,13] The functions ln $A(T)$ appear to deviate from linearity at $T < 77.3$ K, for representative series [Fig. 2(*b*)], which is reminiscent of the nearly constant trend detected for iron proteins at $T < 10$ K.[23]

Averaged hyperfine parameters, over the T ranges investigated, are given in Table 2. The isomer shift and nuclear quadrupole splitting values in each system are practically temperature invariant, which implies the absence of phase transitions.[24] Analogous trends are observed for the linewidths, Table 2; the line asymmetry detected for $Sn^{IV}R_2$–DNA condensates, and the consequent assumption of the occurrence of two tin sites, will be discussed later.

The functions ln $A_t(T)$ and ln $f_a^{rel}(T)$ for alkyltin(IV)–DNA condensates, Figs. 2 and 3 of the present work, essentially correspond to those for low-molecular-weight organotin(IV) salts and complexes.[25] Analogously, the dynamics of ^{57}Fe in iron proteins reflects those of iron salts and complexes at below the transition temperature.[26] In the present context, the slopes d ln$(A_t/A_{77.3})$/dT for alkyltin(IV)–DNA condensates, Table 2, are comparable to those for organotin(IV) polymers,[25a,27] while those of the trialkyltin(IV) condensates are located on the monomer–polymer borderline,[25a,28] according to fingerprint assignments,[25a,27] polymerization mainly referring to the extent of intermolecular interactions in the crystalline solids.[25,27] For example, the slopes were -0.95×10^{-2} and -1.28×10^{-2} K^{-1} for the adenosine monophosphate model complexes $SnR_2(AMP)\cdot 2H_2O$ (R = Me or Bu^n), which are assumed to be polymeric.[10] Moreover, the monomer–polymer borderline for $Sn^{IV}R_3$ derivatives, according to the literature, lies approximately between d ln $A_t/dT = -1.39 \times 10^{-2}$ K^{-1} [the five-co-ordinated site, polymeric, in $Me_3Sn(SCH_2CH_2CO_2)$-$SnMe_3$[28a]] and -2.11×10^{-2} K^{-1} {$SnMe_3[O_2P(NHPh)_2]$, oligomeric[28b]}.

Labelling polymeric substrates with organotin(IV) moieties does not imply that the dynamics of the tin nuclei will be comparable to those of the 'polymer' zone referred to above. In fact, the slopes d ln A/dT for poly(*p*-triphenylstannylstyrene) and poly[diphenyl(1,4-divinylbenzene)tin(IV)] are typical of 'monomeric' species; analogously, data for poly[*p*,*p*′-(di-*p*-tolyl-stannanediyl)distyrene] and poly(*p*,*p*′,*p*″,*p*‴-stannanetetrayl-tetrastyrene) do not substantially differ from those for the respective monomers.[29,30] The dynamics of 'molecular' polymers is not expected consistently to differ from those of the related monomers.[31] It would then appear that also in chemical polymers the dynamics of tin nuclei reflect

Table 2 Tin-119 Mössbauer hyperfine parameters, structural information from point-charge model simulations and molecular dynamics data, for organotin(IV)–DNA (calf thymus) condensates

No.[a]	Organotin(IV)–DNA monomer unit[a]	δ_{av}[b]/ mm s^{-1}	ΔE_{av}[c]/ mm s^{-1}	C–Sn–C/° in SnR_2[d] and C–Sn–A/° in SnR_3[d]	Γ_{1av}[e]/ mm s^{-1}		Γ_{2av}[e]/ mm s^{-1}	10^2 d ln($A_t/A_{77.3}$)/ dT[f] (K^{-1})	θ_D[g]/ K
1–3	$SnMe_2$(DNA monomer)$_2$	1.351 (±0.004)	4.206 (±0.021)	180	0.957 (±0.024)		1.088 (±0.035)	−1.220 (0.996)	47.3
	doublet 1[h]	1.392 (±0.007)	4.436 (±0.017)	180		0.823[i] (±0.023)		—	—
	doublet 2[h]	1.217 (±0.022)	3.517 (±0.039)	143		0.802[i] (±0.023)		—	—
4–7	$SnMe_3$(DNA monomer)	1.363 (±0.004)	3.810 (±0.011)	90	0.802 (±0.016)		0.800 (±0.016)	−1.555 (0.989)	53.5
8–13	$SnEt_2$(DNA monomer)$_2$	1.507 (±0.003)	4.167 (±0.012)	180	0.929 (±0.015)		1.204 (±0.016)	−1.250[j] (0.996)	45.9[j]
	doublet 1[h]	1.576 (±0.007)	4.351 (±0.028)	180		0.839[i] (±0.011)		—	—
	doublet 2[h]	1.336 (±0.014)	3.559 (±0.017)	145		0.835[i] (±0.011)		—	—
8, 9	Mössbauer–Zeeman spectra[k]	1.40	+3.77 (η = 0.00)	152		—		—	—
14–16	$SnEt_3$(DNA monomer)	1.495 (±0.004)	3.887 (±0.007)	90	0.879 (±0.011)		0.909 (±0.014)	−2.045[j] (0.993)	44.7[j]
14, 15	Mössbauer–Zeeman spectra[k]	1.44	−3.68 (η = 0.12)	90		—		—	—

[a] Freeze-dried absorber samples, obtained as described in the Experimental section and Table 1; codes and stoichiometries from Table 1. See text (Results and Discussion). [b] Isomer shifts with respect to $CaSnO_3$ at room temperature, averaged over data in the whole temperature range, Fig. 2 and Table 1, with standard error. [c] Nuclear quadrupole splitting, average values, see (*b*). [d] Calculated by point-charge model simulated structures, see text (Results and Discussion); A refers to an axial ligand atom in structures such as **B**, Fig. 4. [e] Full width at half-height of the resonant peaks, at lower and larger velocity than that of the spectrum centroid, respectively; average values, see footnote *b*. [f] Slopes of functions of normalized total areas under the resonant peaks [Lorentzian, $A = (\pi/2)\varepsilon\Gamma$, ε being the percentage resonant effect] *vs.* T; correlation coefficients in parentheses. Average data, concerning all series of $A(T)$ determinations for each condensate of Table 1 in the ranges 77.3 K–T_{max} for each series (see Fig. 2). [g] Debye temperatures, see text (Results and Discussion), calculated from the slopes of the collective ln ($A_t/A_{77.3}$) *vs.* T functions. Data refer to the assumption of the effective vibrating mass corresponding to the stoichiometries in Table 1. [h] Data related to the fitting of the spectra with two doublets; see text, Experimental section and Results and Discussion, and Fig. 1. [i] $\Gamma_1 = \Gamma_2$ imposed by the fitting using the NORMOS program. [j] Calculated with data points at T ≥ 77.3 K. [k] Spectra determined at 22 K in a transverse magnetic field of 4.75 T; see Fig. 5 and text, Experimental section, and Results and Discussion. The asymmetry parameter $\eta = (V_{xx} - V_{yy})/V_{zz}$, $V_{\alpha\alpha}$ being the components of the electric field gradient tensor.

'intermolecular' (*i.e.* interchain) interactions, as advanced for $[-Sn(Bu^n_2)OCH(CCl_3)O-]_n$.[30] Analogously, using ^{57}Fe Mössbauer spectroscopy, the dynamics of synthetic polymers has been interpreted in terms of 'rapidly increasing molecular freedom' above the glass transition temperature;[32] moreover, low-temperature motions (below ≈200 K) in iron proteins are attributed to intermolecular dynamics.[33–35]

In conclusion, from the functions $\ln(A_t/A_{77.3})(T)$ and $\ln f_a^{rel}(T)$ it can be inferred that the dynamics of $Sn^{IV}R_2$–DNA condensates, lyophilized, reflect the occurrence of interstrand interactions (*i.e.* cross-linking between DNA chains), which are missing in SnR_3–DNA condensates. It seems worth mentioning here a possible analogy of $Sn^{IV}R_2$–DNA with Fe–DNA dried specimens, from which room-temperature ^{57}Fe Mössbauer resonant effects [and presumably low slopes d ln A/dT)] have been detected.[36]

Dynamics from the 'Absolute' Recoil-free Fraction and Correlation with the 'Relative' Functions.—The 'absolute' Lamb–Mössbauer factors, f_a^{abs}, were calculated by the procedure previously reported,[22] based upon the recoil-free fraction of the source (from spectra of β-tin absorbers at 77.3 K), as well as on thickness corrections using Lang's approach,[37] equation (3), where t_1, t_2 are the effective absorber thicknesses

$$f_a^{abs} = \frac{t_1 + t_2}{(\pi/2)\Gamma_{nat}\sigma_0 N} \quad (3)$$

related to the areas of the two resonant peaks of the spectra; Γ_{nat} is the natural linewidth of ^{119}Sn, σ_0 the resonant absorption cross-section of ^{119}Sn, and N the number of absorber resonant atoms per cm^2. Lorentzian lineshapes are generally assumed.

From $f_a^{rel,abs}$ functions Debye temperatures can be obtained by using equation (1), and mean-square displacements of the Mössbauer atoms, $\langle x^2 \rangle$, from equation (4), K being the wavevector of the γ rays.

$$f_a = \exp(-K^2\langle x^2 \rangle) \quad (4)$$

The values of f_a^{rel} obtained for linear functions by equation (1), in the Debye approximation, correspond to f_a^{abs} data, equation (3), and the same holds for the related $\langle x^2 \rangle$ data. Variable parameters for the determination of f_a^{abs} are t_i and N. Eventual errors in the t_i estimates are minimized by the procedure employed, involving the ratio of the experimental areas of the spectra recorded for the specimen as well as for β-tin foils;[22] values of N (total) are calculated from the dry weight of the absorber samples and the assumed stoichiometry, as reported in Table 1. It clearly appears that $f_a^{rel,abs}$, as well as the corresponding $\langle x^2 \rangle$, coincide for the DNA condensates spontaneously formed with $Sn^{IV}Me_2$, $Sn^{IV}Et_2$ and $Sn^{IV}Et_3$ by addition of ethanol solutions of the alkyltin chlorides to aqueous DNA, method (I) (see Experimental section), as shown in Fig. 3 for representative series, while sensibly differing for the $Sn^{IV}Me_2$–DNA condensate precipitated by a standard procedure for DNA [method (II), addition of NaCl and EtOH], as well as for all $Sn^{IV}Me_3$–DNA systems (as exemplified in Fig. 3).

The results are ascribed to the stoichiometries assumed for the alkyltin(IV)–DNA condensates, and consequently to the related values of N. Thus, by method (I), the species $SnMe_2$(DNA monomer)$_2$, $SnEt_2$(DNA monomer)$_2$ and $SnEt_3$(DNA monomer) would be obtained (series 1, 2; 8–13; 14–16 in Table 1), according to earlier reports.[8] For the other systems, N has been estimated by equation (3) employing f_a^{rel} data,[38] in place of f_a^{abs}, and the results obtained are reported in Table 1. It clearly appears that the numbers of ^{119}Sn atoms in the $Sn^{IV}Me_2$– and $Sn^{IV}Me_3$–DNA condensates, series 3 and 4–7 (preparation methods II–IV), are much less than the values estimated by 'gravimetry' on the assumption of the formation of species $SnMe_2$(DNA monomer)$_2$ and $SnMe_3$(DNA monomer).

It is concluded that the present data treatment supports the hypothesis of electrostatic bonding of organotin(IV) to DNA phosphates,[8] based also on data for model systems in solution.[9] The electrical charge of the backbone phosphate groups would be entirely neutralized by alkyltin(IV) cations in DNA condensates obtained by method (I), Table 1, while only partially in the remaining systems, where condensates would also consist of sodium salts of DNA or degraded DNA (by H^+). In the case of $Sn^{IV}Me_3$–DNA, the electrical charge and lipophilicity could also play a role.[8] Results analogous to those reported in Table 1 are obtained on the assumption of the occurrence of two water molecules per phosphate residue, in line with the results for dried DNA.[39]

On the basis of the preceding findings, the variable-temperature Mössbauer data were employed to estimate the Debye temperatures θ_D. For this purpose, the $Sn^{IV}R_2$– and $Sn^{IV}R_3$–DNA condensates are considered to behave as Debye solids, and θ_D data are calculated by applying equation (1) in the high-temperature limit ($T \geqslant \theta_D/2$), the parameter M being taken as the effective vibrating mass,[22,40] corresponding to the 'stoichiometric' masses SnR_2(DNA monomer)$_2$ and SnR_3(DNA monomer) (Table 1). The values thus extracted from the collective functions $\ln(A_t/A_{77.3})(T)$, which correspond to $f_a^{rel}(T)$ as far as the slopes are concerned [equation (1)], are reported in Table 2; the order of magnitude corresponds to those for low-molecular-weight organotin(IV) derivatives,[22,41] in line with the slopes d ln A/dT referred to above. In particular, for the model (polymeric) compounds $SnR_2[O_2P(OPh)_2]_2$ (R = Me, Et or Bu^n), calculations using equation (1) and reported d ln A_t/dT values[10] give θ_D = 56.2, 57.1 and 42.3 K, respectively, assuming M = molecular weight; analogously, for the adenosine monophosphate complexes[10] $SnR_2(AMP)\cdot 2H_2O$ (R = Me or Bu^n), θ_D = 65.0 and 52.0 K, respectively, have been obtained. These θ_D values are of the order of those for alkyltin(IV)–DNA condensates (Table 2), the dynamics of which may then be related to vibrations of the units SnR_2(DNA monomer)$_2$ and SnR_3(DNA monomer). It seems worthwhile to recall that the concept of effective vibrating mass in biological molecules has been applied to the dynamics of haemoglobin.[42]

The magnitude of the mean-square displacements of the Mössbauer atoms, $\langle x^2 \rangle$, may give an indication of the extent of polymerization of solid organotin(IV) derivatives.[43] The $\langle x^2 \rangle(T)$ data for alkyltin(IV)–DNA condensates, calculated from $f_a^{rel,abs}$ data using equation (4), and partially shown in Fig. 3, all lie in Sano's 'zone' for monomers and one-dimensional polymers.[43] There is a surprisingly good agreement with $\langle x^2 \rangle(T)$ functions for ^{57}Fe in deoxymyoglobin and in metmyoglobin in the 'solid state' range, $T \leqslant 200$ K,[26,33,38,44,45] which suggests a strictly analogous dynamic behaviour of the ^{57}Fe and ^{119}Sn nuclei in these systems.

The Tin Environment.—Structures **A** and **B**, Fig. 4, have been previously attributed[8] to non-lyophilized organotin(IV)–DNA condensates (in gelled phases) by structure simulations through application of the point-charge model.[25a,46–48] The calculations of the nuclear quadrupole splitting, ΔE, values reported here, using new estimates of the partial quadrupole splitting (p.q.s.) for H_2O in octahedral and trigonal-bipyramidal structures (Fig. 4), are in still better accordance with the related ΔE_{exptl} data.[8] The octahedral site **C** now appears to be as equally probable as **A**, due to the practical coincidence of p.q.s. data for co-ordinated water and phosphate (Fig. 4).

The Mössbauer spectra of SnR_3(DNA monomer) condensates, as determined for gels and dried solids, are similar for a given R group, as shown by the hyperfine parameters δ, ΔE and Γ in Table 2, as well as in the literature in the case of gels.[8] The linewidths Γ are symmetrical for each peak of the two-line

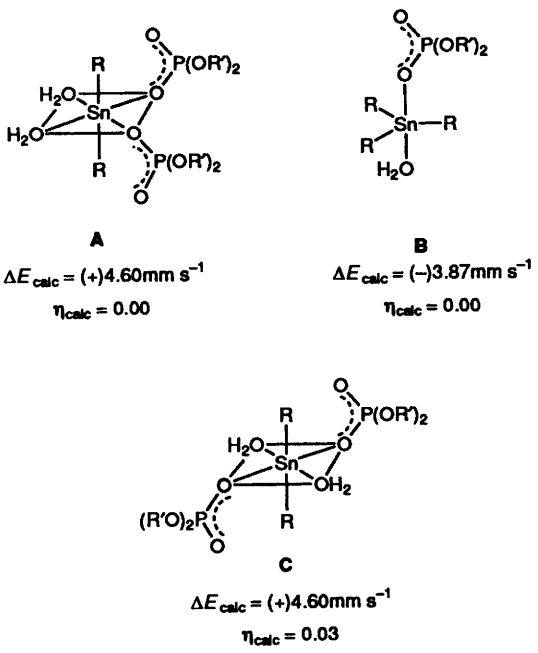

Fig. 4 Point-charge model ('literal' version)[25a,46–48] simulations of the tin environments assumed for SnR_2(DNA monomer)$_2$ and SnR_3(DNA monomer), regular structures. The p.q.s. parameters, mm s^{-1}, employed in the calculation of the nuclear quadrupole splitting parameters, ΔE, as well as of asymmetry parameters $\eta = (V_{xx} - V_{yy})/V_{zz}$,[25a,46–48] are as follows: octahedral configurations **A** and **C**; p.q.s. (R) − p.q.s. (halide) = −1.03;[25a,46,47] p.q.s. $[O_2P(OR')_2]$ − p.q.s. (halide) = +0.11;[9] p.q.s. (H_2O) − p.q.s. (halide) = +0.13 {this work, calculated from[49] ΔE_{expt} = 4.64 mm s^{-1} for $[SnMe_2(H_2O)_4]^{2+}$ in frozen solution at pH 0.95, on the basis of the reported *trans*-octahedral structure[50]}. Trigonal-bipyramidal configuration **B**; p.q.s. $(R)^{eq}$ = −1.13;[48] p.q.s. $[O_2P(OR)_2]^{ax}$ = +0.13;[9] p.q.s. $(H_2O)^{ax}$ = +0.11 {calculated from[49] ΔE_{expt} = (−)3.83 mm s^{-1} for $[SnMe_3(H_2O)_2]^+$, in frozen solution at pH 1.7–3.1); ax = axial, eq = equatorial

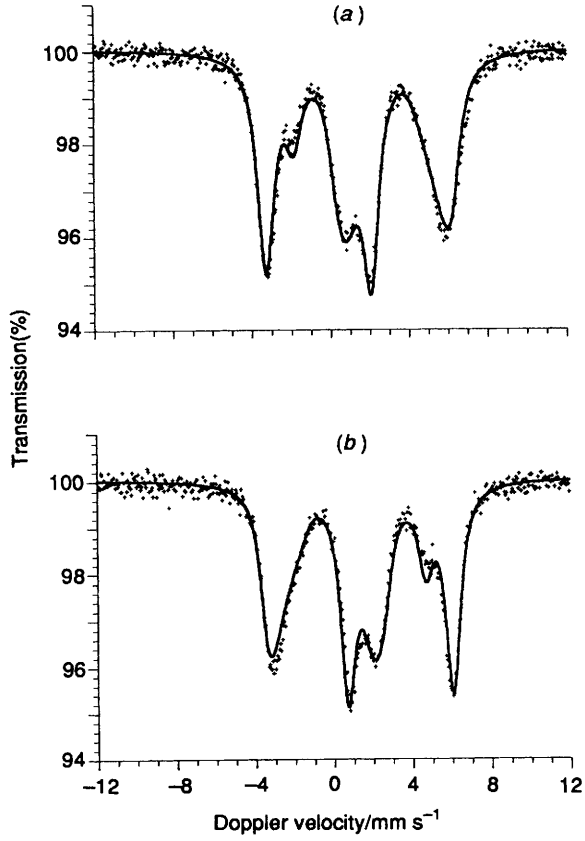

Fig. 5 Mössbauer–Zeeman spectra recorded at 22 K in a transverse magnetic field of 4.75 T. The corresponding parameters, δ, (sign)ΔE and value of η, are in Table 2. (*a*) $SnEt_2$(DNA monomer)$_2$, (*b*) $SnEt_3$(DNA monomer)

spectra, and the respective areas under the two resonant peaks are practically coincident [see *e.g.* the values of ε in the footnotes to Table 4 in ref. 8(*b*)]. A single type of tin site is thus present in these condensates, with structure **B**, Fig. 4, according to a point-charge model simulation.

The spectra of SnR_2(DNA monomer)$_2$ are different. Symmetrical peaks occur for the gels [$\Gamma_1 = \Gamma_2$, Table 3 of ref. 8(*b*)], asymmetrical for the dried specimens ($\Gamma_1 < \Gamma_2$, Table 2 of this work, for fitting of the spectra with one doublet, two peaks); consequently, ΔE_{expt} for dried condensates, Table 2, are less than the values for gels.[8b] Structure **A** or **C** may be generally assumed to occur, the difference $|\Delta E_{expt} - \Delta E_{calc}|$ being around 0.4 mm s^{-1} for the dried compounds (Table 2 and Fig. 4), according to the literature.[46]

These structural assignments are substantially in accord with the data extracted from the Mössbauer–Zeeman[15] spectra in Fig. 5. The value and sign of ΔE for $SnEt_3$(DNA monomer), Table 2, correspond to data calculated for structure **B** in Fig. 4; for $SnEt_2$(DNA monomer)$_2$, the sign of ΔE and the value of η in Table 2 coincide with those from calculations for structures **A** and **C**, the Mössbauer–Zeeman $|\Delta E|$ being, on the other hand, sensibly less than ΔE_{calc}.

The nature of the tin environments in lyophilized SnR_2(DNA monomer)$_2$ may be examined on the assumption of the occurrence of two tin sites, owing to the asymmetry of the Γ parameters for fits with one Lorentzian doublet. The experimental spectra are better fitted by two symmetric doublets, shown in Fig. 1, each describing a tin co-ordination site. It is clear that the ΔE values for the larger doublets (labelled as doublet 1 in Table 2) are strictly comparable to the ΔE data for gelled condensates,[8] so that structures **A** and **C**, Fig. 4, are assigned to these tin sites. The ΔE values for the second site, doublet 2 in Table 2, are in the borderline zone between those for trigonal-bipyramidal SnR_2A_3 species, with equatorial alkyls, and for *trans*-R_2 octahedral SnR_2A_4 (A = donor atom other than carbon), according to fingerprint criteria.[51] The octahedral structure is preferred on the following grounds: (*i*) the octahedral lower fingerprint limit[51] is ΔE = 3.64 mm s^{-1}, quite near to the ΔE data for doublets 2 in Table 2; (*ii*) the trigonal-bipyramidal species SnR_2A_3 would be characterized by negative ΔE values,[47] contrary to the positive sign of ΔE determined here for $SnEt_2$(DNA monomer)$_2$ by Mössbauer–Zeeman spectroscopy (Table 2). The magnitude of ΔE for doublets 2 could be then ascribed to deviations from the regular *trans*-octahedral structure, essentially concerning the CSnC skeleton, which may be estimated by point-charge model simulations considering only the contribution of the Sn–C bond electrons to the electric field gradient tensor.[25a,52] By this procedure, doublets 2 would reflect distorted structures of type **A** or **C**, Fig. 4, with C–Sn–C bond angles of 143 and 145°, respectively, for the $Sn^{IV}Me_2$ and $Sn^{IV}Et_2$ moieties; regular structures **A**–**C** would occur for all other tin sites (Table 2).

The peak asymmetry referred to above in connection with the freeze-dried condensates SnR_2(DNA monomer)$_2$ could also originate, in principle, from the Goldanskii–Karyagin effect, which has been detected in a series of organotin(IV) derivatives.[53] We are inclined to exclude this in the present context, since functions A_+/A_- *vs.* T (where A_+, A_- are the areas under the resonant peaks at larger and lower velocities than that of the spectrum centroid, respectively, in spectra fitted with two Lorentzian lines) do not show a definite temperature dependence, contrary to literature reports.[53]

Conclusion

Deoxyribonucleic acid (DNA) condensates[54] are formed by the addition of alkyltin(IV) chlorides in ethanol solution [$SnR_2Cl_2(EtOH)_2$ (R = Me or Et) and $SnEt_3Cl(EtOH)$, the related cationic species also being present[8]] to aqueous native DNA (calf thymus); the charge of the backbone phosphodiester groups would be neutralized by alkyltin(IV) cations, the latter then being included in the gelled phases and abstracted from solution equilibria, avoiding the formation of hydrolysis products.[55] Methyltin(IV) cations appear to compete with H^+ and Na^+ in the neutralization of DNA phosphate; the electrical charge on the tin atoms, as well as the lipophilicity of the radicals bound to the metal, seem to play a role in the condensation processes.[8] The alkyltin(IV) moieties in the condensates would be co-ordinated by oxygen atoms from phosphodiester residues and from water molecules, analogous to metal ion–nucleic acid interactions [*e.g.* as detected for aquated Mg^{2+} and 'RNA, where $Mg(H_2O)_4(phosphodiester)_2$ units have been identified[56]]. The tin environments appear to be *trans*-dialkyl octahedral in $Sn^{IV}R_2$–DNA condensates; two sites would occur, characterized by regular and distorted (in the CSnC skeleton) structures, respectively. Regular trigonal-bipyramidal structures with equatorial SnC_3 groups, in an unique site, would be present in $Sn^{IV}R_3$–DNA. Assuming the occurrence of toroidal condensates,[57] it can be speculated that $Sn^{IV}R_3$ moieties are appended to the phosphodiester backbone,[8] while $Sn^{IV}R_2$ would bridge phosphodiester groups within the toroids through interstrand bonding (which is consistent with structural parameters[57b,58]). The transition from B- to A- and C-DNA upon lyophilization, with the consequent change in the number of water molecules per nucleotide,[58] would play a role in the formation of two distinct co-ordination sites at tin in $Sn^{IV}R_2$–DNA. Moreover, one of the sites could also originate through tin co-ordination by two vicinal phosphodiester groups. Further studies are clearly needed in this context.

The dynamics of tin nuclei in alkyltin(IV)–DNA condensates (freeze-dried) is comparable to motions in organotin(IV) salts and complexes, as inferred by analogy of the functions $\ln A(T)$, $f_a^{rel,abs}(T)$, $\langle x^2 \rangle(T)$ and θ_D, on the assumption of modes involving molecular groups bound to the metal atom. The observed linear temperature functions suggest a harmonic behaviour, such as determined for proteins at $T < \approx 200$ K.[33,34,59] The relevant motions would take place at characteristic times less than 17.86 ns (the lifetime of 23.8 KeV ^{119}Sn), the amplitudes lying around 0.01–0.02 nm (as extracted from the $\langle x^2 \rangle$ data, see *e.g.* the values in Fig. 3). The latter are in the range characteristic for a number of internal motions in nucleic acids [Table 3.1, p. 29, of ref. 1 (*b*)], including those related to molecular groups such as bases in double helices. The assumption that the dynamics of alkyltin(IV)–DNA condensates reflects motions related to the interactions of tin nuclei with the surface of DNA double strands, involving tin–mononucleotide groups, thus appears to be reliable.

References

1 See, for example, (*a*) *Structure and Dynamics of Nucleic Acids, Proteins and Membranes*, eds. E. Clementi and S. Chin, Plenum, New York, London, 1986; (*b*) J. A. McCammon and S. C. Harvey, *Dynamics of Proteins and Nucleic Acids*, Cambridge University Press, Cambridge, 1987.
2 T. M. Alam and G. P. Drobny, *Chem. Rev.*, 1991, **91**, 1545.
3 R. Giegè, P. V. Huong and D. Moras, *Spectrochim. Acta, Part A*, 1986, **42**, 387.
4 B. H. Robinson, G. Forgacs, L. R. Dalton and H. L. Frisch, *J. Chem. Phys.*, 1980, **73**, 4688; B. H. Robinson, L. S. Lerman, A. H. Beth, H. L. Frisch, L. R. Dalton and C. Auer, *J. Mol. Biol.*, 1980, **139**, 19; E. J. Hustedt, A. Spaltenstein, J. J. Kirchner, P. B. Hopkins and B. H. Robinson, *Biochemistry*, 1993, **32**, 1774.
5 H. Castleman, L. S. Specthrie, L. Makowski and B. F. Erlander, *J. Biomol. Struct. Dyn.*, 1984, **2**, 271.
6 D. L. Beveridge and G. Ravishanker, *Curr. Opinion Struct. Biol.*, 1994, **2**, 246 and refs. therein.
7 K. C. Molloy, in *The Chemistry of the Metal–Carbon Bond*, ed. F. R. Hartley, Wiley, New York, London, 1989, ch. 11, p. 465.
8 (*a*) R. Barbieri and A. Silvestri, *J. Inorg. Biochem.*, 1991, **41**, 31; (*b*) R. Barbieri, A. Silvestri, A. M. Giuliani, V. Piro, F. Di Simone and G. Madonia, *J. Chem. Soc., Dalton Trans.*, 1992, 585; (*c*) V. Piro, F. Di Simone, G. Madonia, A. Silvestri, A. M. Giuliani, G. Ruisi and R. Barbieri, *Appl. Organomet. Chem.*, 1992, **6**, 537.
9 R. Barbieri, A. Silvestri and V. Piro, *J. Chem. Soc., Dalton Trans.*, 1990, 3605.
10 R. Barbieri, G. Alonzo and R. H. Herber, *J. Chem. Soc., Dalton Trans.*, 1987, 789.
11 J. Laudát and F. Laudát, *Europhys. Lett.*, 1992, **20**, 663.
12 F. Parak, M. Fischer, E. Graffweg and H. Formanek, in *Structure and Dynamics of Nucleic Acids, Proteins and Membranes*, eds. E. Clementi and S. Chin, Plenum, New York, London, 1986, p. 139.
13 S. G. Cohen, E. R. Bauminger, I. Nowik, S. Ofer and J. Yariv, *Phys. Rev. Lett.*, 1981, **46**, 1244.
14 See, for example, E. R. Bauminger, I. Nowik, S. Ofer and C. Heitner-Wirguin, *Polymer*, 1985, **26**, 1829.
15 R. L. Collins and J. C. Travis, in *Mössbauer Effect Methodology*, ed. I. J. Gruverman, Plenum, New York, 1967, vol. 3, p. 123.
16 J. G. A. Luijten and G. J. M. van der Kerk, *Investigations in the Field of Organotin Chemistry*, Tin Research Institute, Greenford, Middlesex, 1955.
17 R. E. Ingham, S. D. Rosenberg and H. Gilman, *Chem. Rev.*, 1960, **60**, 459.
18 R. H. Herber and S. Chandra, *J. Chem. Phys.*, 1970, **52**, 6045; H. A. Stöckler and H. Sano, *Nucl. Instrum. Methods*, 1966, **44**, 103.
19 A. Baldini, F. Cecconi, F. Del Giallo, F. Pieralli and G. Spina, *Hyperfine Interact.*, 1990, **58**, 2649.
20 G. Longworth, in *Mössbauer Spectroscopy Applied to Inorganic Chemistry*, ed. G. J. Long, Plenum, New York, London, 1984, vol. 1, p. 43.
21 E. Kolk, in *Dynamical Properties of Solids*, eds. G. K. Horton and A. A. Maradudin, North Holland, Amsterdam, 1984, vol. 5, p. 5.
22 R. Barbieri, A. Silvestri, L. Pellerito, A. Gennaro, M. Petrera and N. Burriesci, *J. Chem. Soc., Dalton Trans.*, 1980, 1983, and refs. therein.
23 A. Dwivedi, T. Pederson and P. G. Debrunner, *J. Phys. (Paris)*, 1979, **40**, C2-531.
24 See, for example, R. S. Preston, in *Mössbauer Isomer Shifts*, eds. G. K. Shenoy and F. E. Wagner, North Holland, Amsterdam, 1978, ch. 6a, pp. 292 and 293.
25 (*a*) R. V. Parish, in *Mössbauer Spectroscopy Applied to Inorganic Chemistry*, ed. G. J. Long, Plenum, New York, 1984, vol. 1, pp. 527–575 and refs. therein; (*b*) K. C. Molloy and K. Quill, *J. Chem. Soc., Dalton Trans.*, 1985, 1417 and refs. therein.
26 See, for example, K. H. Mayo, D. Kucheida, F. Parak and J. C. W. Chien, *Proc. Natl. Acad. Sci. USA*, 1983, **80**, 5294.
27 R. Barbieri, A. Silvestri, A. Barbieri, G. Ruisi, F. Huber and C.-D. Hager, *Gazz. Chim. Ital.*, 1994, **124**, 187.
28 (*a*) R. Barbieri, A. Silvestri, F. Huber and C.-D. Hager, *Inorg. Chim. Acta*, 1981, **55**, L13; (*b*) K. C. Molloy and T. G. Purcell, *J. Organomet. Chem.* 1986, **312**, 167.
29 K. C. Molloy, J. J. Zuckerman, H. Schumann and G. Rodevald, *Inorg. Chem.*, 1980, **19**, 1089.
30 R. Barbieri, L. Pellerito, A. Silvestri, G. Ruisi and J. G. Noltes, *J. Organomet. Chem.*, 1981, **210**, 43.
31 H. A. Stöckler and H. Sano, *Chem. Commun.*, 1969, 954.
32 D. C. Champency and D. F. Sedgwick, *Chem. Phys. Lett.*, 1972, **15**, 377.
33 E. N. Frolov, M. Fischer, E. Graffweg, M. A. Mirishly, V. I. Goldanskii and F. G. Parak, *Eur. Biophys. J.*, 1991, **19**, 253.
34 F. Parak and G. U. Nienhaus, *J. Non-Cryst. Solids*, 1991, **131–133**, 362.
35 F. Parak, K. Achterhold, H. Hartmann, J. Heinzl, E. Huenges and G. U. Nienhaus, *Hyperfine Interact.*, 1992, **71**, 1319.
36 A. A. Kochanska-Dziurowicz, T. Wilczok and Z. Dzierzewicz, *Stud. Biophys.*, 1987, **122**, 201.
37 G. Lang, *Nucl. Instrum. Methods*, 1963, **24**, 425.
38 F. Parak, E. N. Frolov, R. L. Mössbauer and V. I. Goldanskii, *J. Mol. Biol.*, 1981, **145**, 825; F. Parak, E. W. Knapp and D. Kucheida, *J. Mol. Biol.*, 1982, **161**, 177.

39 M. Falk, K. A. Hartman, jun., and R. C. Lord, *J. Am. Chem. Soc.*, 1962, **84**, 3843; 1963, **85**, 387, 391.
40 R. H. Herber, in *Chemical Mössbauer Spectroscopy*, ed. R. H. Herber, Plenum, New York, London, 1984, pp. 199–216.
41 S. Matsubara, M. Katada, K. Sato, I. Motoyama and H. Sano, *J. Phys. (Paris)*, 1979, **40**, C2-263.
42 A. Levy, *Biochemistry*, 1989, **28**, 7144.
43 H. Sano and Y. Mekata, *Chem. Lett.*, 1975, 155.
44 F. Parak, J. Heidemeier and G. U. Nienhaus, *Hyperfine Interact.*, 1988, **40**, 147.
45 F. Parak, M. Fischer and G. U. Nienhaus, *J. Mol. Liquids*, 1989, **42**, 145.
46 M. G. Clark, A. G. Maddock and R. H. Platt, *J. Chem. Soc., Dalton Trans.*, 1972, 281.
47 G. M. Bancroft and R. H. Platt, *Adv. Inorg. Chem. Radiochem.*, 1972, **15**, 59.
48 G. M. Bancroft, V. G. Kumar Das, T. K. Sham and M. G. Clark, *J. Chem. Soc., Dalton Trans.*, 1976, 643.
49 R. Barbieri and A. Silvestri, *Inorg. Chim. Acta*, 1991, **188**, 95.
50 I. Hippel, P. G. Jones and A. Blaschette, *J. Organomet. Chem.*, 1993, **448**, 63.
51 M. T. Musmeci, G. Madonia, M. T. Lo Giudice, A. Silvestri, G. Ruisi and R. Barbieri, *Appl. Organomet. Chem.*, 1992, **6**, 127 and refs. therein.
52 T. K. Sham and G. M. Bancroft, *Inorg. Chem.*, 1975, **14**, 2281.
53 See, for example, R. H. Herber and S. Chandra, *J. Chem. Phys.*, 1970, **52**, 6045; 1971, **54**, 1847.
54 G. S. Manning, *Q. Rev. Biophys.*, II, 1978, **2**, 179.
55 See, for example, M. J. Hynes and M. O'Dowd, *J. Chem. Soc., Dalton Trans.*, 1987, 563.
56 M. M. Teeter, G. J. Quigley and A. Rich, in *Nucleic Acid–Metal Ion Interactions*, ed. T. G. Spiro, Wiley, New York, 1980, ch. 4, p. 145.
57 (*a*) K. A. Marx, *NATO ASI Ser. E*, 1987, **133**, 137; (*b*) P. G. Arscott, A. Z. Li and V. A. Bloomfield, *Biopolymers*, 1990, **30**, 619; (*c*) V. A. Bloomfield, *Biopolymers*, 1991, **31**, 1471.
58 W. Saenger, *Principles of Nucleic Acid Structure*, Springer, New York, Berlin, 1984.
59 S. Cusack and W. Doster, *Biophys. J.*, 1990, **58**, 243.

Received 27*th July* 1994; *Paper* 4/04603J